applied sciences

MDPI

Article

A Depth-Bistatic Bottom Reverberation Model and Comparison with Data from an Active Triplet Towed Array Experiment

Youngcheol Jung [1], Woojae Seong [1], Keunhwa Lee [2,*] and Seongil Kim [3]

1 Department of Naval Architecture and Ocean Engineering/RIMSE, Seoul National University, Seoul 08826, Korea; dicaffri@snu.ac.kr (Y.J.); wseong@snu.ac.kr (W.S.)
2 Department of Defense Systems Engineering, Sejong University, Seoul 05006, Korea
3 Agency for Defense Development; Jinhae 51678, Korea; sikim@add.re.kr
* Correspondence: nasalkh2@sejong.ac.kr; Tel.: +82-02-3408-3508

Received: 30 March 2020; Accepted: 27 April 2020; Published: 28 April 2020

Featured Application: Sonar system.

Abstract: In this paper, a depth-bistatic bottom reverberation model that employs the ray theory is presented. The model can be applied to an active towed array in the ocean. The reverberation time series are modeled under the depth-bistatic assumption and their Doppler shift is calculated based on the actual source–receiver geometry. This model can handle $N \times 2D$ range-dependent bathymetry, the geometry of a triplet array, and the Doppler motion of the source, targets, and receiver. The model predictions are compared with the mid-frequency reverberation data measured by an active triplet towed array during August 2015 in the East Sea, Korea. These data are collected with a variable depth source at mid-frequency and the triplet line array in a deep-water environment. Model predictions of the beam time series and its spectrogram are in good agreement with the measurement. In particular, we discuss the effects of the source and receiver depths on the reverberation in deep water observed in both the measured and modeled results.

Keywords: active triplet towed array; bottom reverberation; East sea experiment; time-spectral signal processing

1. Introduction

Ocean reverberation is generated by the scattering mechanism of ocean boundary irregularities and medium inhomogeneities [1] and is one of the dominant environmental factors that have to be considered in the design of active sonar systems [2–5].

Since the 1940s, there have been many studies on the prediction of reverberation in the ocean [6–9]. These studies can be categorized in a variety of ways, e.g., physics of scattering, coherence, scattering modeling, propagation modeling, and geometry of sources and receivers. In terms of propagation modeling, reverberation models are usually classified into energy flux models [10,11], ray-based models [12–15], normal mode models [16], and parabolic equation models [17]. Among them, the ray-based model is known to be well-suited for reverberation modeling of the complex ocean environment in the frequency range of 1 to 10 kHz.

The numerical burdens of reverberation modeling are generally high because the modeling is performed with the repetitive usage of the propagation model and the scattering model along each scattering element of a physical domain [15]. In the case of bistatic sonar, where the source and receiver are separated by a distance, the numerical burden will be even higher, because out-of-plane scattering

is included in the calculation [18]. However, such a rigorous approach may be unnecessary for an active towed array where the distance between the source and receiver is not large (<1 km).

In this study, we extend the 2D geometrical ray-bundle reverberation model for the fixed mono-static sonar [14] to a 3D environment with the approach and develop a depth-bistatic bottom reverberation model for an active towed array composed of a variable depth source and a triplet line array. This model neglects out-of-plane scattering in the sea floor but allows for bistatic Doppler shift, which is simplified as a straight-line propagation between a moving source, a moving receiver, and fixed scatterers. A major advantage of this depth-bistatic scheme is that it can reduce the computational costs. The fully bistatic scheme basically requires two independent ray-bundle (or ray-beam) tracings for a bottom cell because the source and receiver is located on the out-of-plane, while the depth-bistatic scheme uses one ray-bundle tracing in a plane where the bottom cell, the range, and the receiver are located. When the distance between the source and receiver is small, the latter has the similar accuracy as the former in the long-range reverberation.

Moreover, we confirm the validity of the proposed model using mid-frequency reverberation data [19] collected in the East Sea of Korea during August 2015 by the Agency for Defense Development of Korea. These data are valuable in two aspects. One aspect is that they were obtained with a variable depth source in the mid-frequency range of 2 to 4 kHz in a deep-water environment. Another aspect is to use the triplet array, which can resolve the left/right ambiguity [20,21]. This enables a detailed analysis of a coherent reverberation signal in the azimuth. Note that the state-of- the-art reverberation experiments are well described by Yang et al. in [9].

This paper is organized as follows: Section 2 describes a depth-bistatic bottom reverberation model with a moving source and receiver for a complex bathymetry. In Section 3, an overview of our reverberation experiment and the signal processing method are presented. Some observations for the azimuth and the operation depths from the measured data are described. Section 4 includes the model-data comparisons. Finally, Section 5 contains a summary and conclusions.

2. Depth-Bistatic Bottom Reverberation Model

The active towed array system of this study consists of a depth variable source and a triplet line array, operated with cable in a research vessel. The operation depths of the source and receiver arrays can be controlled by the ship speed and the employed cable length. The geometry of this array is nominally considered bistatic. However, the range between the source and receiver arrays in our system is usually within 1 km. This small range suggests the applicability of the depth-bistatic model, which takes into account that the source and receiver are collocated in range but separated in depth, in order to predict the reverberation of an active towed array.

Reverberation in the ocean is expressed as the sum of the time signals scattered from the randomly distributed scatterers in volume and boundary. It means that the reverberation signal is essentially a random process. To model a random pressure signal directly is numerically expensive and meaningless. Thus, a heuristic approach for modeling the ensemble-averaged intensity signal has been widely used in the underwater acoustics community [22].

We consider an $N \times 2D$ ocean environment with a depth-bistatic geometry of the source and receiver, as shown in Figure 1. Assuming the positions of the source and receiver are fixed, the impulse response of the incoherent bottom reverberation for the i-th bottom cell is formulated with the approach of [14] as the following equation:

$$h^i_{nm}(t) = \Delta\phi\Delta\tau_{nm}\left|p_n\right|^2\left|p_m\right|^2\sigma(\theta_n,\theta_m)\prod(\frac{t-\tau_n-\tau_m}{\Delta\tau_{nm}}), \quad (1)$$

where $\Delta\phi$ is the azimuthal interval, the subscripts n and m indicate the eigenray index from the source to the scatterer and from the scatterer to the receiver, respectively, $p_{n,m}$ and $\tau_{m,n}$ are the propagation losses and the time delays for a one-way path, respectively, and σ is the bottom scattering cross-section as a function of the incident angle θ_n and the scattered angle θ_m. In addition, $\Delta\tau_{nm}$ is defined as

$\Delta\tau_{nm} = (\Delta R/c_0)(\cos\theta_n + \cos\theta_m)$ with a range interval ΔR and a sound speed c_0 near the bottom. $\prod(t)$ is a rectangular function defined as 1 inside −1/2 to 1/2 and 0 outside it. Note that Equation (1) is called the ensemble-averaged impulse response.

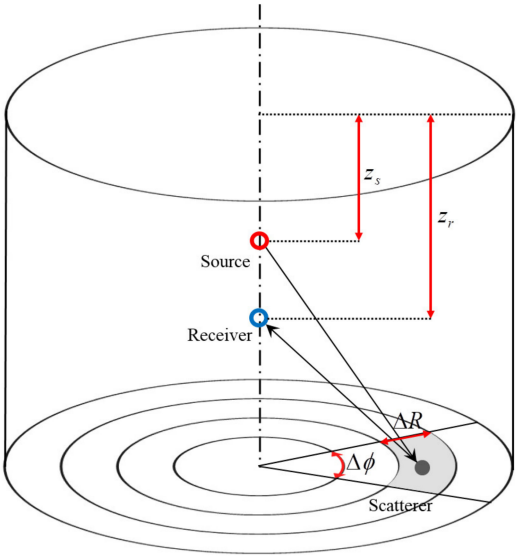

Figure 1. Schematic of the $N \times 2D$ bottom reverberation modeling of the depth-bistatic geometry.

To account for Doppler effects resulting from the motions of the source and receiver, we apply a Doppler shift obtained from the straight-line propagation between the source, receiver, and the i-th bottom cell into Equation (2). The Doppler angular frequency is written as:

$$\omega_{d,i} = \omega \frac{c_r + \vec{V}_{r,i} \cdot \vec{n}_{r,i}}{c_t - \vec{V}_{t,i} \cdot \vec{n}_{t,i}}, \tag{2}$$

where ω is the original angular frequency of the transmitted waveform, c_r and c_t are the sound speeds in the receiver and the source positions, respectively, and $\vec{V}_{r.i}$ and $\vec{V}_{t,i}$ are the velocities of the receiver and the source relative to the i-th scatterer, respectively. Here, $\vec{n}_{r,i}$ and $\vec{n}_{t,i}$ are the unit vectors in the direction of the receiver to the i-th scatterer and in the direction of the source to the scatterer, respectively. For example, supposing that the source position is $\vec{r}_t = [r_b \sin\phi_t, r_b \cos\phi_t, z_s]$, the receiver position is $\vec{r}_r = [0, 0, z_r]$, and the scatterer position is $\vec{r}_s = [R\sin\phi, R\cos\phi, z_b]$; $\vec{n}_{r,i}$ and $\vec{n}_{t,i}$ are defined as $\vec{n}_{r,i} = (\vec{r}_r - \vec{r}_s)/\left|\vec{r}_r - \vec{r}_s\right|$ and $\vec{n}_{t,i} = (\vec{r}_t - \vec{r}_s)/\left|\vec{r}_t - \vec{r}_s\right|$, respectively.

If the Doppler angular frequency within a bottom cell is stationary during the pulse duration, the Doppler-shifted impulse response can easily be calculated with Equation (2) as

$$h^i_{d,nm}(t) = h^i_{nm}(\alpha t), \tag{3}$$

where:

$$\alpha = \frac{c_r + \vec{V}_{r,i} \cdot \vec{n}_{r,i}}{c_t - \vec{V}_{t,i} \cdot \vec{n}_{t,i}}. \tag{4}$$

Equation (3) is the Doppler-shifted impulse response at the 2D cell of the bottom bathymetry for a moving depth-bistatic array. However, it turns out that a direct use of Equation (3) does not work well for efficient reverberation modeling. This is because the Doppler angular frequency is truly stationary in a bottom cell with a small range step of ΔR. To solve this problem, we apply an interpolation method for Doppler modeling. First, the values of α in all bottom cells along the range in an azimuthal slice are

calculated using Equation (4). Then, the linear interpolation is used to generate new samples between the original values of α using the sampling frequency of the reverberation signal. With this procedure, the α within a bottom cell becomes time varying, which increases the accuracy of Equation (3) even for a large range step.

The total reverberation signal is defined according to the intensity of the source pulse $I_0(t)$ as:

$$I(t) = I_0(t) * \sum_i \sum_n \sum_m h^i_{d,nm}(t). \quad (5)$$

Here, the summation index i indicates the number of the bottom cell, and the indexes of n and m are the number of incident and scattered eigenrays at the i-th bottom cell, respectively.

3. Sea Experiment in the East Sea

3.1. Overview

On 20–21 August 2015, an experiment was conducted in the East Sea of Korea to measure the ocean bottom reverberation using an active triplet towed array. The experiment site was located off the coast of Pohang city, which is in the east-southern region of East Sea, as shown in Figure 2a. The water depth varies, approximately between 500 to 1500 m. The state of the sea was calm, and the wind speed was between 1.7 and 2.8 m/s, so we expect that the surface reverberation was small. The research vessel (R/V) Cheong-Hae towed a variable depth source and a triplet towed receiver array, a nested array consisting of 96 triplets as shown in Figure 3.

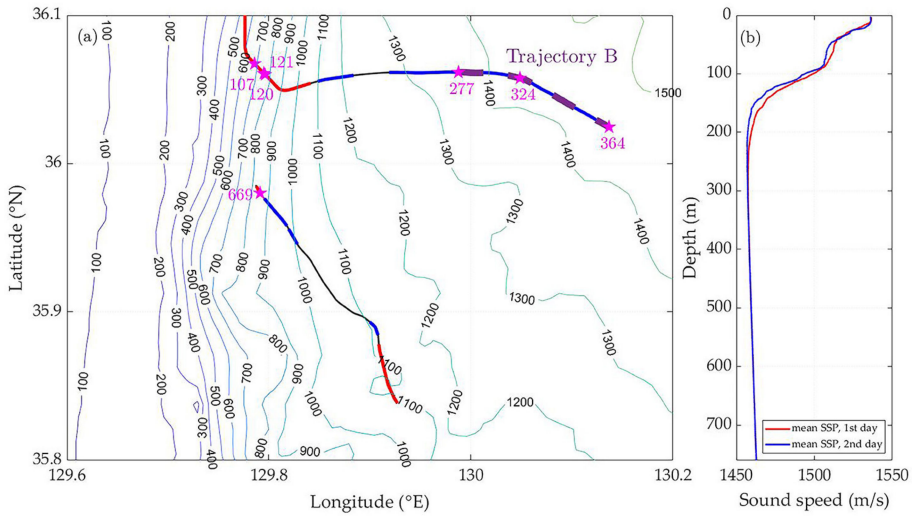

Figure 2. Sea trial environment for the measurement of ocean reverberation in the East Sea, Korea. (**a**) Trajectory of the research vessel at the experimental site. The symbols of red circles and blue crosses indicate the positions where the CW pings and the LFM pings are launched, respectively. The pentagram symbols and the "Trajectory B" denote the positions of the pings used for the analysis. (**b**) Mean sound speed profiles of the first and second days.

The trajectories of the research vessel are displayed in Figure 2a. Although a total of five types of source waveforms were used in the experiment, we analyzed only two waveforms, namely, the continuous wave (CW) and the linear frequency modulation (LFM). Their center frequency is 3 kHz. The CW used has pulse durations of 0.1, 0.3, and 1 s, respectively. The bandwidths of the LFM were set to 400 Hz, 1 kHz, and 2 kHz. For two days, a total of 678 pings (364 pings on the first day, 314 pings on the second day) were launched. Among them, the number of CW pings was 265 and the number of LFM pings was 273.

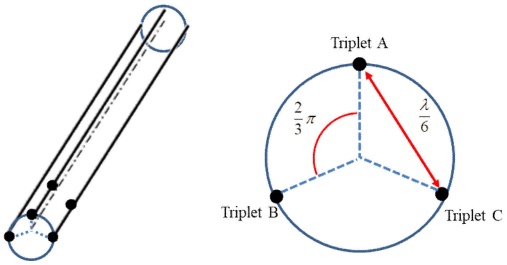

Figure 3. Structure of the triplet towed array where λ is the wavelength of design frequency.

The sound speed profile was acquired with expendable bathythermographs (XBTs). Figure 2b shows the mean sound speed for each day and we see that the minimum sound speed depth was observed between 226 m and 274 m. For this deep-water sound speed, the bottom-reflected wave is dominant. The ocean sediment at the experimental site consists of fine silt and clay corresponding to a mean grain size M_z of 7Φ to 10Φ.

During the experiment, the operation depth of the source and receiver varied. Figure 4a shows the mean depth of the source and receiver and their ping number. The operating depth of the source and receiver was between 4 to 240 m on the first day, and 4 to 74 m on the second day. Figure 4b represents the mean tow speed of the research vessel.

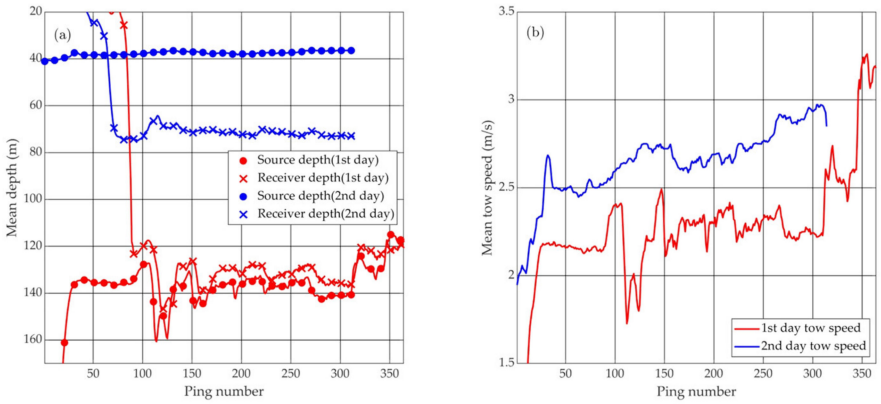

Figure 4. (**a**) Mean operation depth of the source and receiver array for each ping number. (**b**) Mean tow speed of the research vessel for each ping number. The true ping number on the second day is the nominal ping number shown on the *x*-axis of each figure plus 314.

3.2. Signal Processing

For coherent processing, we apply a time-domain beamforming into the acquired sensor data. The conventional beamforming method is used for both triplet beamforming and line array beamforming [20,21]. The time delay error due to the rolling of the triplets is compensated with the roll data measured by 18 roll sensors spaced at equal intervals throughout the array aperture. The beam data is sampled in time with a sampling frequency of 15,360 Hz. The flow chart of the coherent processing is given in Figure 5.

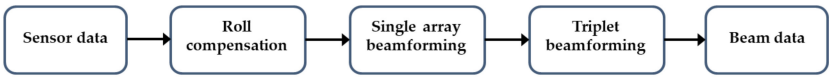

Figure 5. Flow chart of triplet array processing.

For the time-frequency analysis, we produce the spectrograms of each sensor data and beam data with a window size of 1 s for the Hanning window and a 50% overlap. To pick the tonal in the spectrogram, the instantaneous frequency estimation method [23] is used as follows:

$$f_{inst}(t) = \frac{\int_{-\infty}^{\infty} fP(t,f)df}{\int_{-\infty}^{\infty} P(t,f)df}, \tag{6}$$

where $P(t,f)$ is the spectrogram function at time t and frequency f.

3.3. Data Analysis

Figure 6 shows an example of the reverberation data. The time origin indicates the time at which the sound wave begins to emanate from the source. The horizontal axis indicates time and the vertical axis indicates the sensor number for each line array. We choose two different results using the same CW with a 3 kHz center frequency and 1 s duration in a similar bathymetry (See Figure 2). The upper figures show the reverberation acquired on the first day at a source depth of 127 m and a receiver array depth of 117 m (ping 107), and the reverberation of the lower figures are measured at a source depth of 36 m and a receiver array depth of 72 m (ping 669). As shown in Figure 6, the reverberation time of the lower figure is shorter.

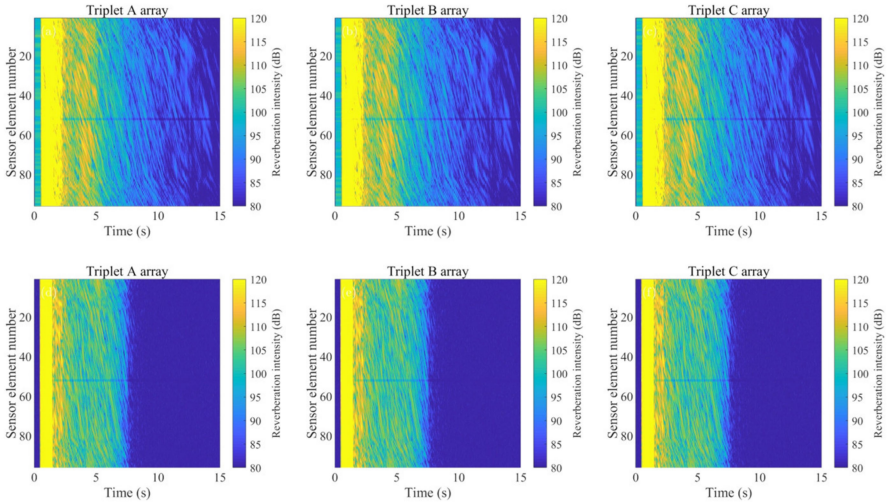

Figure 6. Two examples of the measured CW reverberation intensity for the time and sensors of each line array in the triplet line array. The upper figures are the results of ping 107 (z_s = 127 m and z_r = 117 m) and the lower figures are those of ping 669 (z_s = 36 m and z_r = 72 m).

This result is related to wave propagation physics in deep water. We simulate a ray tracing for the above two source depths and plot it in Figure 7. The bathymetry is set to be flat and the sound speed profile of Figure 2b is used. In Figure 7, the field of the bottom-reflected rays is more spread as the source depth is deeper. This is the reason for the longer reverberation time in the upper figures of Figure 6. In addition, we observed some striation patterns for the sensor number (array length) due to the ship speed.

To analyze the dependency of the array depth on the reverberation in more detail, we observe the beam time signal measured in "trajectory B" of Figure 2. Along this trajectory, a total of 88 LFM pings with a 3 kHz center frequency, a 1 kHz bandwidth, and 1 s duration are launched while varying the source and receiver depths. Figure 8 shows the beam time series from the starboard direction for the ping numbers. The reverberation time for the ping number varies accordingly as the source and receiver depths are varied.

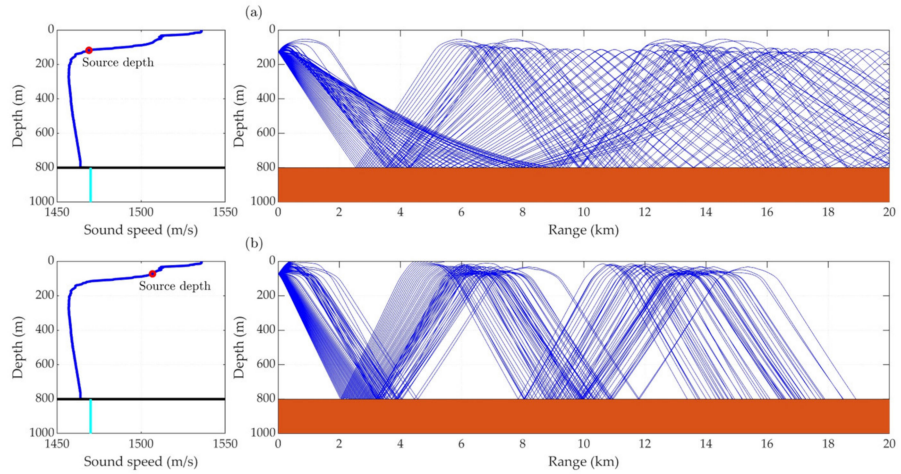

Figure 7. Ray propagation according to source depth. (**a**) z_s = 127 m, (**b**) z_r = 36 m.

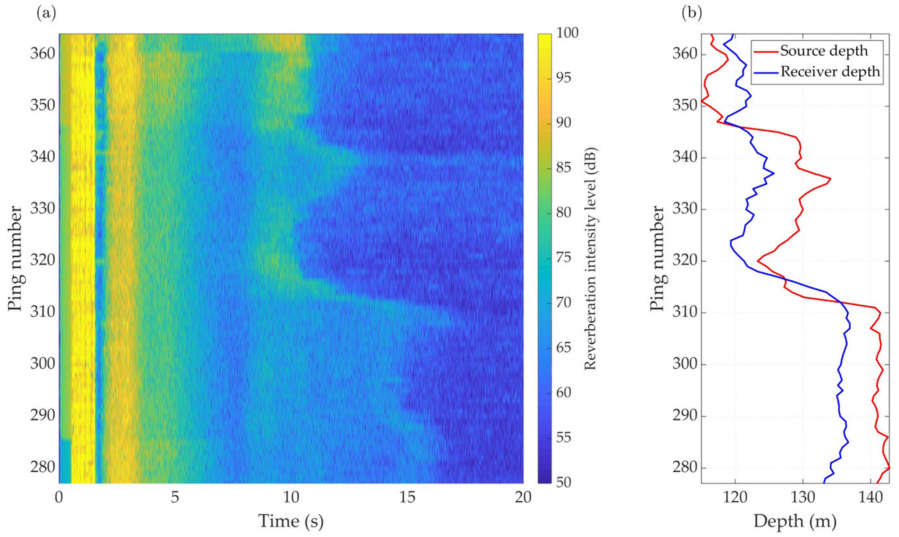

Figure 8. (**a**) Beam time series for the time and ping number from starboard direction. (**b**) Source and receiver depth corresponding to the ping number.

In Figure 9, we compare two beam time series measured at a continental slope at a depth of 500 m (ping 107) and at a deep ocean floor with a depth of 1000 m (ping 324), respectively. The source and array depths are similar in both cases. Ping 107 is a CW with a 3 kHz center frequency and 1 s duration and ping 324 is LFM with the same center frequency and duration, and a 1 kHz bandwidth. For the early region of the beam time series, time signals with a large amplitude are clipped. At a glance, the dependency of reverberation time for the relative beam angle is different in two figures. Since the duration of the source pulse is the same at both pings, it is presumed that this tendency is mainly due to the varying bottom bathymetry. The continental slope region has a range and azimuth-dependent bathymetry; however, the deep ocean floor region is deeper and relatively range-independent.

Figure 10 shows an example of spectrograms of the CW with a 3 kHz center frequency and 0.1 and 1 s durations. These are the spectrograms of the sensor data that were generated by ping 120 and ping 121. The horizontal axis indicates the frequency shift. Interestingly, a broadening of the tonal energy can clearly be observed. Such a broadening comes from the Doppler effect of the moving source and receiver and the fixed scatterers. Recently, Hefner and Hodgkiss [24] have reported a similar phenomenon through the observation of a reverberation spectrum of TREX 13 data and modeled it in the Pekeris waveguide using a mapping technique.

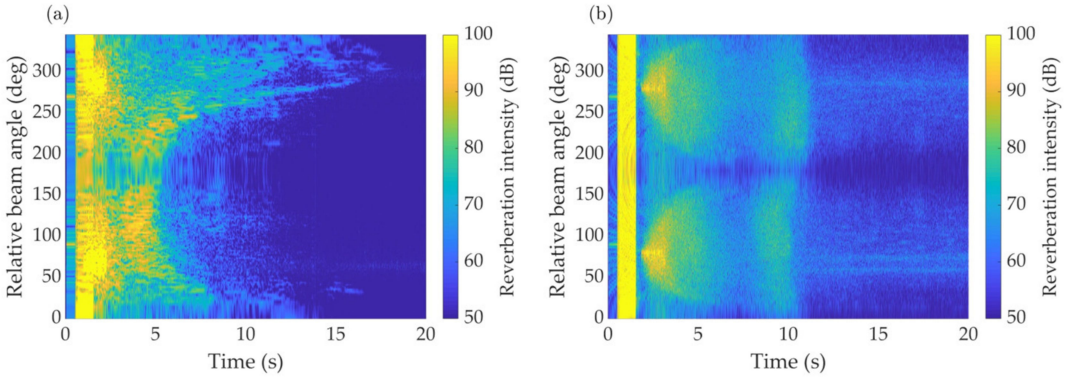

Figure 9. Beam time series at two different sites for the time and relative beam angle measured clockwise from the bow direction. (**a**) Ping 107 (CW ping, pulse duration 1 s, z_s = 135 m, z_r = 129 m), and (**b**) ping 324 (LFM ping, pulse duration 1 s, bandwidth 1 kHz, z_s = 135 m, z_r = 129 m).

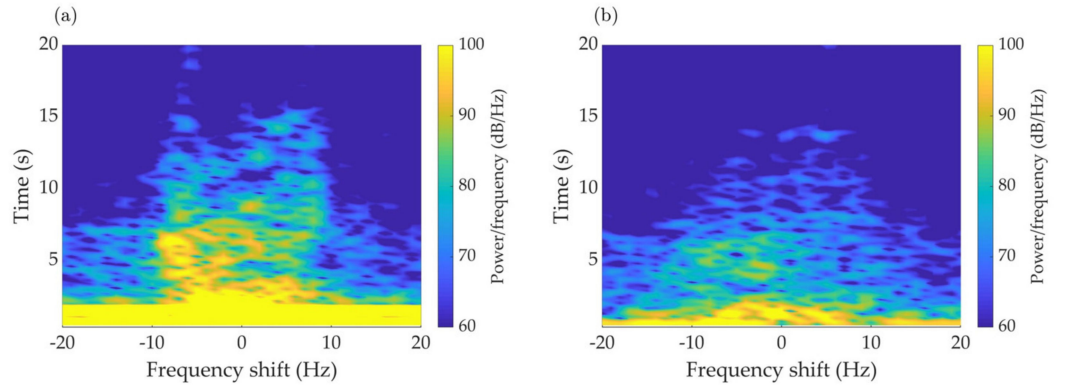

Figure 10. Spectrogram of data received at a single particular sensor in the event of CW ping 120 and CW ping 121. (**a**) Pulse duration 1 s, (**b**) Pulse duration 0.1 s.

4. Model/Data Comparison

A comparison of the modeled data and the measured data is shown in this section. For the reverberation modeling, the empirical Lambert's law scattering function with kernels [25] was used as given by:

$$\sigma(\theta_n, \theta_m) = \mu(\sin\theta_n)^p(\sin\theta_m)^q, \tag{7}$$

where μ is the empirical Lambert's coefficient and p and q are scattering kernels. We set Lambert's coefficient μ to be −40 dB for CW and −37 dB for LFM. Two scattering kernels are chosen to be 0.5 through data fitting. The sea-floor bathymetry is created using the General Bathymetric Chart of the Oceans (GEBCO) with a 15 arc-second resolution grid (~450 m) [26]. The properties of the ocean bottom are obtained from the geological database of the co-located sediment coring. The sound speed of the surficial sediment is 1470 m/s, its density is 1200 kg/m^3, and the attenuation coefficient is 0.08 dB/λ, which corresponds to silt-clay sediment. The bottom is regarded as a homogeneous half-space. Finally, for a realistic simulation, the ambient noise signal of a white Gaussian noise type is added to the sensor data.

Figure 11 shows the modeled reverberations of ping 107 and 324, described in Section 3. The results of Figures 9 and 11 show very similar features. In Figure 11a, a longer reverberation time is observed for the downslope direction than for the upslope direction. To examine this feature precisely, the beam time series shown in Figure 11a is sliced at starboard and port, which corresponds to the upslope and the downslope directions, respectively.

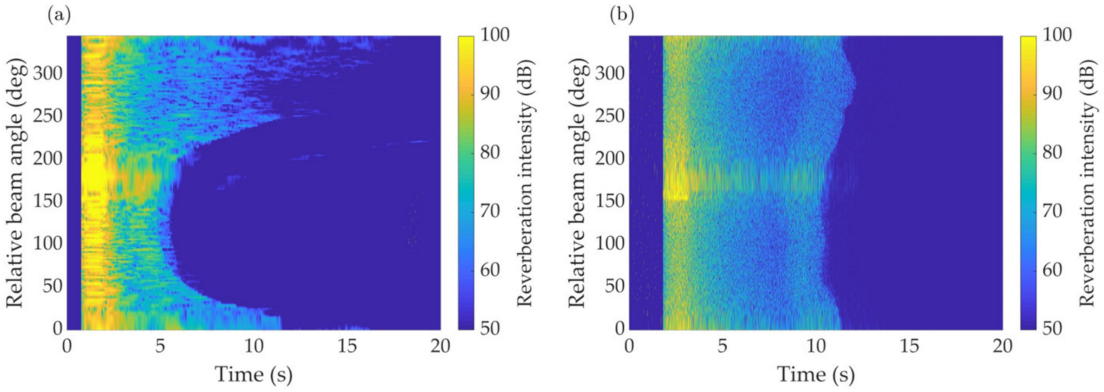

Figure 11. Modeled beam time series. (**a**) Ping 107 (CW reverberation) and (**b**) ping 324 (LFM reverberation).

Figure 12 shows the results. To remove the random fluctuation of the reverberation, the measured data were time-averaged with the window of 0.06 s. The dotted line indicates a noise floor of 40 dB and 60 dB, respectively. In the starting region of measured data, ghost signal is observed by the electric coupling of source and receiver array. After about 0.5 s, the direct blast is arrived. We note again that the time signal with a large voltage are clipped. For the case of ping 107 that the water depth is shallower, it is seen that the direct blast is mixed with multi-path signals and reverberation signals. Totally, the modeled results (solid line) agree well with the measured results (dashed line), except that a longer tail appears in the latter. This tail may be a consequence of the scattering from sea-floor layering or volume inhomogeneity.

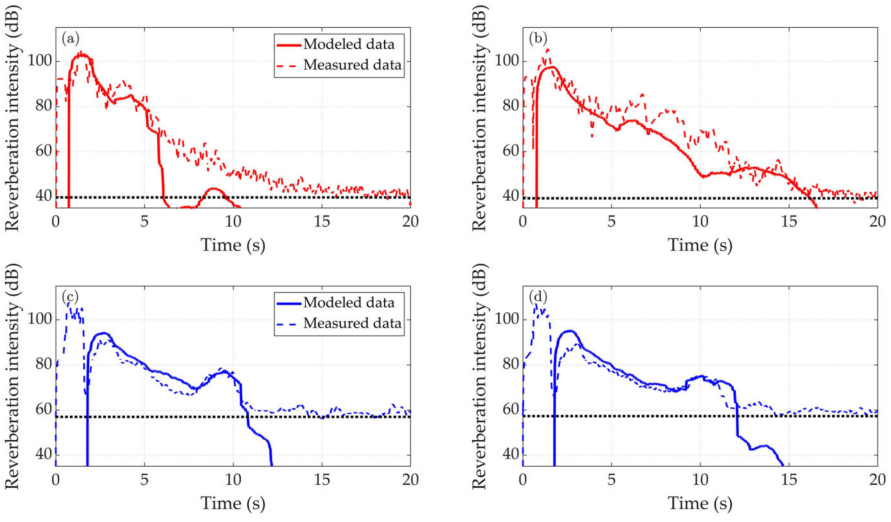

Figure 12. Comparison of the modeled reverberation intensity and the data at both broadsides for ping 107 and ping 324. (**a**) 90° for ping 107, (**b**) 270° for ping 107, (**c**) 90° for ping 324, and (**d**) 270° for ping 324.

In Figure 13, the modeled spectrogram for the CW with the 1 s duration and 3 kHz center frequency is given and compared with the results obtained without the platform motion. The environmental parameters used are the same as for Figure 11. Comparing Figures 10a and 13a, it is clear that our model describes the spectrum broadening well. In Figure 13b, we can see that the model without Doppler correction fails to predict realistic reverberation.

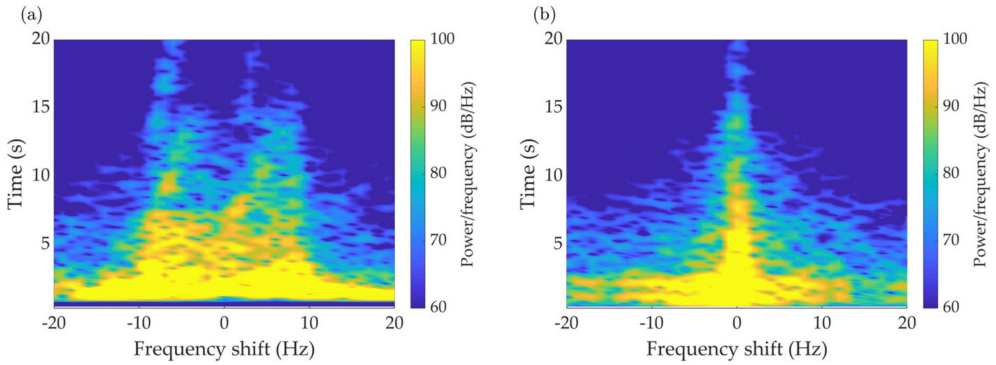

Figure 13. Modeled spectrogram using the data information of Figure 10a. (**a**) Considering the platform motion and (**b**) not considering the platform motion.

Finally, Figure 14 shows the change of the extracted Doppler shift for the motion of the source and receiver arrays using Equation (6). The reverberation data of ping 120 with a 3 kHz center frequency and a 1 s duration is chosen. The extracted Doppler shift fluctuates due to contamination by multi-path scattering at an early time and the time variability of the towed system and environment, while the overall trend is clearly revealed. We compare it with the Doppler shift extracted from the modeled reverberation using Equation (6) again. The red solid line shows the results without a correction of the bistatic geometry, which means that the range of the source and receiver is zero. The blue solid line represents the results with the true bistatic geometry. It can be seen that the use of the bistatic geometry is better for predicting the Doppler shift of the CW reverberation in the active towed array system than that of a depth-bistatic geometry.

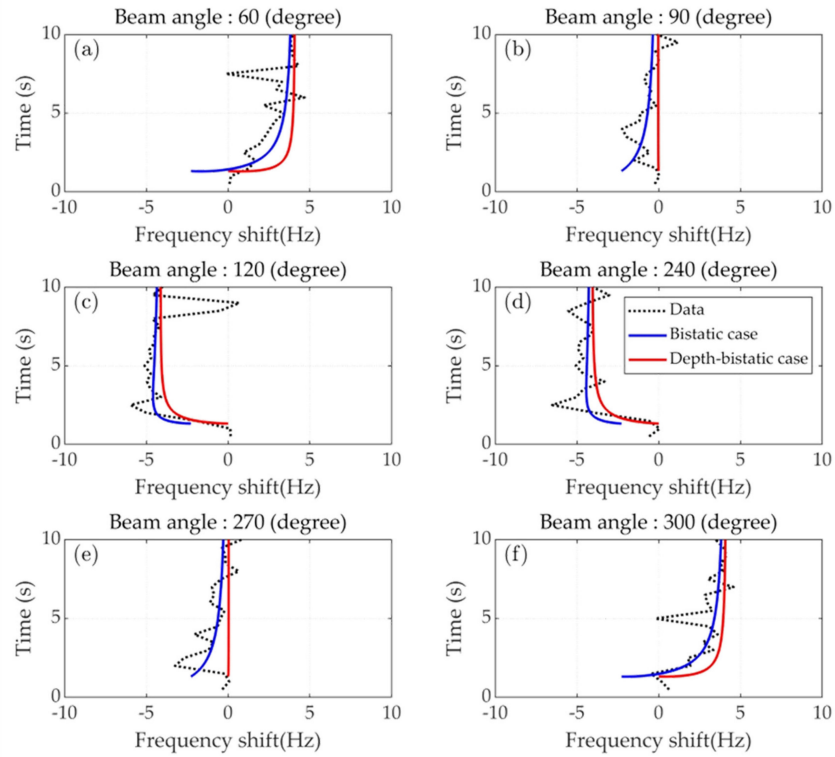

Figure 14. Comparison of the modeled Doppler shift and the extracted Doppler shift from data for six relative beam directions at ping 120. The black dotted line indicates the extracted result. The blue solid line and the red solid line indicate the modeled result of a bistatic geometry and of a depth-bistatic geometry. (**a**) 60°, (**b**) 90°, (**c**) 120°, (**d**) 240°, (**e**) 270°, and (**f**) 300°.

5. Conclusions

We have developed an $N \times 2D$ bottom reverberation model for the depth-bistatic sonar which is useful for an active towed array system. This model an extension of a previously published geometric ray-bundle reverberation model for a moving, depth-bistatic sonar. The main assumption is to neglect all out-of-scattering between the source, scatterer, and receiver in the bistatic geometry. This is valid when the distance between the source and receiver is small, as in the active towed array sonar system.

With this depth-bistatic model, the reverberation data acquired in the East Sea of Korea with the active triplet towed array system are analyzed. The experimental conditions at the time were favorable for us to obtain high-quality bottom-reverberation data. From the measured data, we first observe the effect of the operation depth on the bottom reverberation in deep water. Second, the beam data analysis shows that the reverberation pattern at an azimuth is strongly dependent on its bathymetry. Moreover, the Doppler broadening and shifting caused by the moving platform can be observed with a time-frequency analysis.

Some of the measured data are compared with the modeled data in the time, frequency, and beam domains. Our model favorably describes the key features observed in the real reverberation data, such as the variability of the reverberation with the operation depth, the bathymetry, the steering direction, and the Doppler effect. One limitation of this study is the lack of consideration for multi-path arrivals in the calculation of the Doppler angular frequency, which is noticeable in the near field reverberation. This factor should be included in future works on the fully bistatic model.

Author Contributions: Conceptualization, S.K. and W.S.; methodology and software, Y.J. and K.L.; validation, K.L. and W.S.; data acquisition, S.K.; writing—original draft preparation, Y.J. and K.L.; writing—review and editing, K.L. and W.S. All authors have read and agreed to the published version of the manuscript.

Funding: This work was supported by the Agency for Defense Development in Korea under Contract No. UD190005DD.

Acknowledgments: The institute of Engineering Research at Seoul National University provided research facilities for data processing in this work.

Conflicts of Interest: The authors declare no conflict of interest.

References

1. Ol'shevskii, V.V. *Characteristics of Sea Reverberation*; Consultants Bureau: New York, NY, USA, 1967; pp. 1–38.
2. Princehouse, D.W. REVGEN, a real time reverberation generator. In Proceedings of the ICASSP '77 IEEE International Conference on Acoustics, Speech, and Signal Processing, Hartford, CT, USA, 8–11 May 1977; pp. 827–835.
3. Hodgkiss, W.S. An oceanic reverberation model. *IEEE J. Ocean. Eng.* **1984**, *9*, 63–72. [CrossRef]
4. Chamberlain, S.G.; Galli, J.C. A model for numerical simulation of nonstationary sonar reverberation using linear spectral prediction. *IEEE J. Ocean. Eng.* **1983**, *8*, 21–36. [CrossRef]
5. Luby, J.C.; Lytle, D.W. Autoregressive modeling of nonstationary multibeam sonar reverberation. *IEEE J. Ocean. Eng.* **1987**, *12*, 116–129. [CrossRef]
6. Preston, J.R. Reverberation at the Mid-Atlantic ridge during the 1993 ARSRP experiment seen by R/V Alliance from 200–1400 Hz and some modeling inferences. *J. Acoust. Soc. Am.* **2000**, *107*, 237–259. [CrossRef] [PubMed]
7. Preston, J.R.; Abraham, D.A. Non-Rayleigh reverberation characteristics near 400 Hz observed on the New Jersey shelf. *IEEE J. Oceanic Eng.* **2004**, *29*, 215–235. [CrossRef]
8. Ellis, D.D.; Yang, J.; Preston, J.R.; Pecknold, S. A normal mode reverberation and target echo model to interpret towed array data in the target and reverberation experiments. *IEEE Oceanic Eng.* **2017**, *42*, 344–361. [CrossRef]
9. Yang, J.; Tang, D.; Hefner, B.T.; Williams, K.L.; Preston, J.R. Overview of midfrequency reverberation data acquired during the target and reverberation experiment 2013. *IEEE Oceanic Eng.* **2018**, *43*, 563–585. [CrossRef]

10. Harrison, C.H. Closed-form expressions for ocean reverberation and signal excess with mode stripping and Lambert's law. *J. Acoust. Soc. Am.* **2003**, *114*, 2744–2756. [CrossRef] [PubMed]
11. Harrison, C.H. Fast bistatic signal to reverberation ratio calculation. *J. Comput. Acoust.* **2005**, *13*, 317–340. [CrossRef]
12. Weinberg, H.; Keenan, R.E. Gaussian ray bundles for modeling high frequency propagation loss under shallow-water conditions. *J. Acoust. Soc. Am.* **1996**, *100*, 1421–1431. [CrossRef]
13. Keenan, R. An introduction to GRAB eigenrays and CASS reverberation and signal excess. In Proceedings of the MTS/OCEANS 2000 Conference, Providence, RI, USA, 11–14 September 2000; pp. 1065–1070.
14. Lee, K.; Chu, Y.; Seong, W. Geometrical ray-bundle reverberation modeling. *J. Comput. Acout.* **2013**, *21*, 135011. [CrossRef]
15. Choo, Y.; Seong, W.; Lee, K. Efficient algorithm for long-range monostatic reverberation in shallow water using geometrical ray-bundle. *J. Comput. Acoust.* **2014**, *21*, 1450005. [CrossRef]
16. Ellis, D.D. A shallow-water normal-mode reverberation model. *J. Acoust. Soc. Am.* **1994**, *97*, 2804–2814. [CrossRef]
17. Lingevitch, J.F.; Fromm, D.M.; LePage, K.D. Parabolic equation technique for reverberation modeling. *J. Acoust. Soc. Am.* **2007**, *122*, 3074. [CrossRef]
18. Etter, R.C. *Underwater Acoustic Modeling and Simulation*, 3rd ed.; Spon Press: New York, NY, USA, 2003; pp. 255–257.
19. Lee, K.; Seong, W.; Kim, S. Estimation of the roll angle in a triplet towed array using oceanic surface-generated ambient noise. *J. Acoust. Soc. Am.* **2017**, *142*, EL123–EL129. [CrossRef] [PubMed]
20. Georgios, H.; Baldacci, A. Unambiguous triplet array beamforming and calibration algorithms to facilitate an environmentally adaptive active sonar concept. In Proceedings of the IEEE Oceans 2006, Boston, MA, USA, 19–21 September 2006; pp. 479–484. [CrossRef]
21. Hughes, D.T. *Aspects of Cardioid Processing*; Saclant Undersea Research Centre: La Spezia, Italy, 2000; SACLANTCEN-SR-329.
22. Jackson, D.; Richardson, M. *High.-Frequency Seafloor Acoustics*; Springer: New York, NY, USA, 2007; pp. 7–28. [CrossRef]
23. Boashash, B. Estimating and interpreting the Instantaneous frequency of a signal—Part 1: Fundamentals. *Proc. IEEE* **1992**, *80*, 520–538. [CrossRef]
24. Hefner, B.T.; Hodgkiss, W.S. Reverberation due to a moving, narrowband source in an ocean waveguide. *J. Acoust. Soc. Am.* **2019**, *146*, 1661–1669. [CrossRef] [PubMed]
25. Holland, C.W. Constrained comparison of ocean waveguide reverberation theory and observations. *J. Acoust. Soc. Am.* **2006**, *120*, 1922–1931. [CrossRef]
26. General Bathymetric Chart of the Oceans (GEBCO) (2019), GEBCO_2019 grid. Available online: http://www.gebco.net (accessed on 15 December 2019).